nature structural & molecular biology

SR protein kinases promote splicing of nonconsensus introns

Jesse J Lipp[1,3], Michael C Marvin[2,3], Kevan M Shokat[1] & Christine Guthrie[2]

Phosphorylation of the spliceosome is essential for RNA splicing, yet how and to what extent kinase signaling affects splicing have not been defined on a genome-wide basis. Using a chemical genetic approach, we show in *Schizosaccharomyces pombe* that the SR protein kinase Dsk1 is required for efficient splicing of introns with suboptimal splice sites. Systematic substrate mapping in fission yeast and human cells revealed that SRPKs target evolutionarily conserved spliceosomal proteins, including the branchpoint-binding protein Bpb1 (SF1 in humans), by using an RXXSP consensus motif for substrate recognition. Phosphorylation of SF1 increases SF1 binding to introns with nonconsensus splice sites *in vitro*, and mutation of such sites to consensus relieves the requirement for Dsk1 and phosphorylated Bpb1 *in vivo*. Modulation of splicing efficiency through kinase signaling pathways may allow tuning of gene expression in response to environmental and developmental cues.

The spliceosome is an evolutionarily conserved RNA–protein complex that identifies and catalytically removes intronic sequences from precursor mRNA (pre-mRNA). Recognition of introns of diverse lengths and sequences requires a cooperative and dynamic network of interactions between mRNA transcripts and the splicing machinery[1]. The assembly of the spliceosome and the subsequent catalysis of the splicing reaction requires a cycle of phosphorylation and dephosphorylation[2–4]. Such phosphorylation events are attributed to evolutionarily conserved kinases of the SR protein kinase (SRPK)[5–7], the Cdc2-like kinase (CLK)[8,9] and the PRP4 kinase families[10]. Phosphorylation primarily occurs at repeats of serine-arginine (SR) dipeptides[11], which commonly occur in spliceosomal proteins and their regulators[12–14]. Studies analyzing the effects of phosphorylation of the splicing machinery have used elegant reporter constructs and *in vitro* assays to establish the functional importance of spliceosome phosphorylation for constitutive and alternative splicing[15–20]. Moreover, recent work including chemical inhibition of the CLK kinase family[21] and short interfering RNA–mediated knockdown of SRPK upon stimulation by epidermal growth factor[22] has demonstrated that loss of kinase activity affects the splicing of a subset of introns. Given the important role of splicing kinases, it is vital to deduce the basic rules and patterns of how splicing kinase signaling affects RNA splicing on a genome-wide level.

In this study, we take a chemical genetic approach in the fission yeast *S. pombe* to show that the SR protein kinase Dsk1 promotes efficient splicing of introns with noncanonical splice sites *in vivo*. Using a substrate mapping screen, we identify direct targets of Dsk1 and its human ortholog Srpk2. We also show that phosphorylation of two conserved sites of the branchpoint-binding protein Bpb1 increases Bpb1's capacity to bind to suboptimal branchpoint sequences *in vitro* and that this phosphorylation is crucial for efficient splicing of introns with nonconsensus splice sites *in vivo*.

RESULTS

Activity of Dsk1 and Prp4 promotes splicing efficiency

We constructed analog-sensitive (denoted with '-as') *S. pombe* strains for each ortholog of the three major human splicing kinase families: Dsk1 (SRPK), Lkh1 (CLK) and Prp4 (PRP4). Analog-sensitive alleles allow the specific inhibition of kinase activity with a bulky ATP-competitive inhibitor[23] (validation in **Fig. 1a** and **Supplementary Fig. 1a–c**). To monitor the functional consequences of splicing kinase inhibition on the genome-wide splicing pattern, we grew wild-type (WT) and analog-sensitive *dsk1*, *prp4* and *lkh1* strains in the presence of 10 μM 3-BrB-PP1 (4-amino-1-*tert*-butyl-3-(3-bromobenzyl)pyrazolo[3,4-*d*]pyrimidine, denoted 3BrB) and hybridized corresponding samples in a direct two-color design to a custom splicing microarray containing 4,615 introns (**Supplementary Fig. 1d,e**; methodology in ref. 24). Inhibition of Dsk1 and Prp4 caused a significant increase of intron retention in 1,945 (~42%) and 2,148 splicing events (~47%), respectively, thus indicating broad defects in RNA splicing (**Fig. 1b**). Intron retention upon inhibition of Dsk1 and Prp4 affected a similar set of introns (Pearson's $\rho = 0.71 \pm 0.01$ s.e.m.; $P < 10^{-6}$, two sided). The average accumulation of significantly retained introns was ~1.6-fold and ~1.9-fold over control for inhibitor treatment of Dsk1-as and Prp4-as, respectively (**Supplementary Fig. 1f**). A small subset of introns (~2%) displayed enhanced splicing upon kinase inhibition (**Fig. 1b**). Consistently with this, reverse-transcription quantitative PCR (RT-qPCR) of introns 1 and 3 of the *fkh1* gene, which were strongly retained in the microarray analysis, displayed intron accumulation when Dsk1 or Prp4 were inhibited (**Fig. 1c** and **Supplementary Fig. 1g**). Surprisingly, neither inhibition of Lkh1 nor

[1]Department of Cellular and Molecular Pharmacology, Howard Hughes Medical Institute, University of California, San Francisco, San Francisco, California, USA. [2]Department of Biochemistry and Biophysics, University of California, San Francisco, San Francisco, California, USA. [3]These authors contributed equally to this work. Correspondence should be addressed to K.M.S. (kevan.shokat@ucsf.edu) or C.G. (christineguthrie@gmail.com).

Received 19 May; accepted 4 June; published online 13 July 2015; doi:10.1038/nsmb.3057

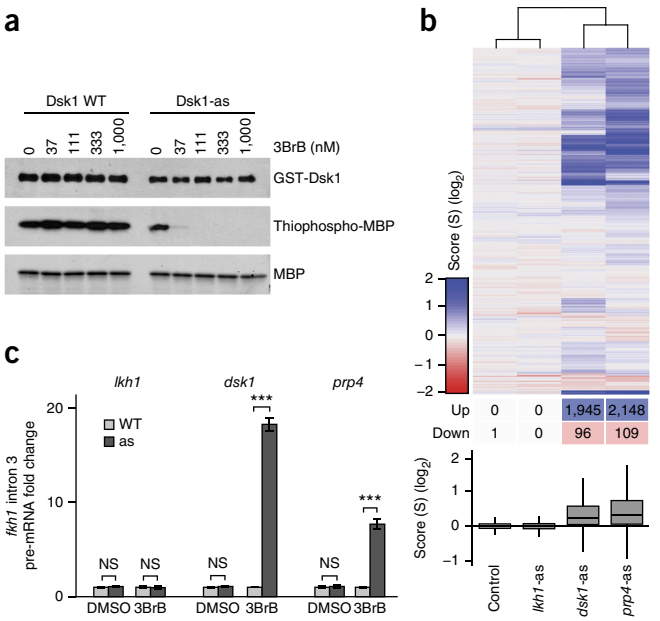

Figure 1 Splicing kinase activity promotes efficient RNA splicing in *S. pombe*. (**a**) Western blot of *in vitro* kinase assay analyzing the thiophosphorylation of myelin basic protein (MBP) by recombinant Dsk1 WT (left) and Dsk1-as (right). Uncropped images are shown in **Supplementary Data Set 1**. GST, glutathione S-transferase tag. (**b**) Top, heat map showing hierarchical clustering of 4,615 splicing events in *S. pombe*. Blue, increased intron retention (up); red, decreased intron retention (down). Middle, total number of significant splicing events (false discovery rate of 5%, Benjamini-Hochberg) for each category. Bottom, box plot representing the distributions of scores for each genotype. Lower and upper boundaries of boxes indicate the 25th and 75th percentiles; the horizontal dividing line shows the median. Scores outside the range of the whiskers (1.5× interquartile range) are omitted. (**c**) Bar graphs displaying the fold enrichment of *fkh1* intron 3 pre-mRNA upon inhibition of the *S. pombe* splicing kinases Dsk1, Lkh1 and Prp4, determined by RT-qPCR. Values are normalized to their respective controls. Error bars, s.e.m. ($n = 3$ cell cultures). NS, $P > 0.05$; ***$P < 0.001$ by two-sided Student's *t* test.

deletion of the *lkh1* gene significantly changed the global splicing pattern (**Fig. 1b** and **Supplementary Fig. 1h**) or the splicing of the *fkh1* gene (**Fig. 1c** and **Supplementary Fig. 1g**). We conclude that Dsk1 and Prp4 kinases have a broad impact on RNA splicing in *S. pombe*, whereas Lkh1 appears to be dispensable under standard growth conditions.

Splicing kinases use a conserved RXXSP phosphorylation motif

Given the important role of splicing kinases in promoting genome-wide RNA splicing, we used a chemical genetic substrate mapping technique to identify their functionally relevant targets[23,25]. In addition to allowing specific inhibition, analog-sensitive kinases allow identification of direct substrates by binding bulky ATP-γS analogs and transferring the terminal thiophosphate to its native substrate. We labeled fission yeast extracts with *N*6-phenethyl-ATP-γS in the presence of either recombinant WT or analog-sensitive Dsk1. We then purified thiophosphorylated peptides and identified 131 direct Dsk1 substrates as well as their phosphorylation sites by MS (**Supplementary Table 1**). A similar set of mapping experiments revealed 73 direct Lkh1 targets (**Supplementary Table 2**). Despite great effort, we were unable to map direct substrates of fission yeast Prp4, owing to the decreased *in vitro* kinase activity resulting from mutation of the gatekeeper residue (F238G).

On the basis of the phosphorylation sites identified in the screen, we determined an empirical consensus motif for Dsk1 (**Fig. 2a**) and Lkh1 (**Fig. 2b**). Both kinases preferred arginines and serines at alternating positions, consistently with the canonical view that splicing kinases phosphorylate sequences rich in RS dipeptide[8,13,26]. Interestingly, arginine at position −3 and proline at position +1 were

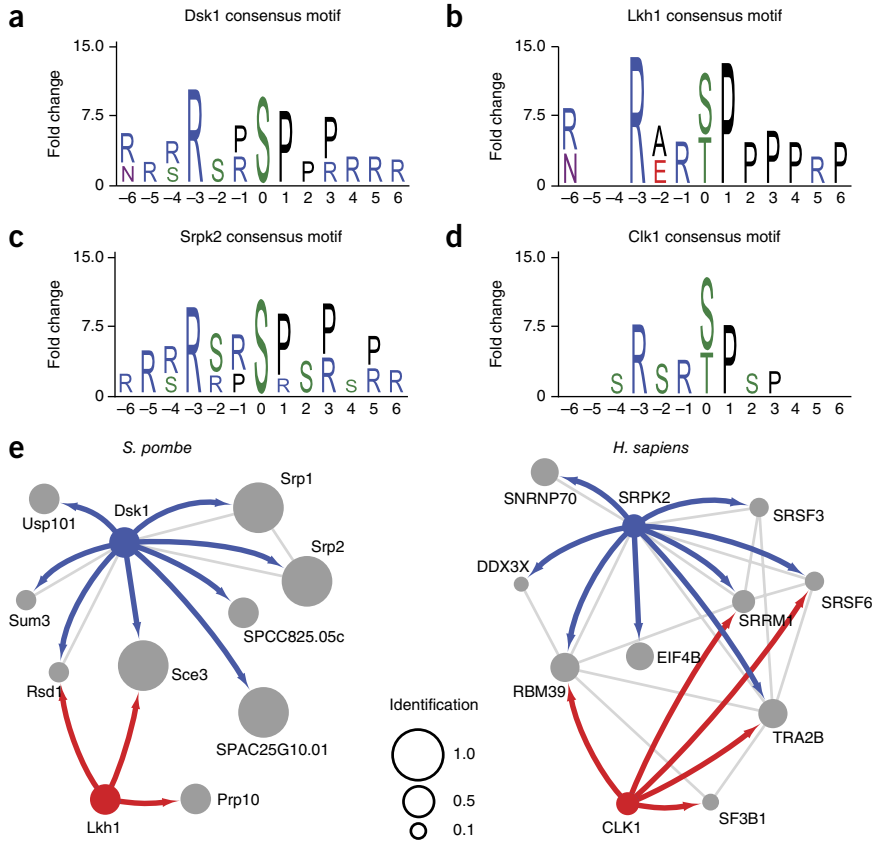

Figure 2 SR protein kinases use an evolutionarily conserved RXXSP motif for substrate recognition. (**a**–**d**) Empirical consensus motifs of the fission yeast kinases Dsk1 (**a**) and Lkh1 (**b**) as well as their human orthologs, Srpk2 (**c**) and Clk1 (**d**), on the basis of phosphorylation sites identified by substrate mapping. Position 0 indicates the site of phosphorylation. Amino acids with highly significant enrichment over genomic background are shown ($P \leq 0.001$; Online Methods). (**e**) Network diagram of a splicing kinase–phosphorylation network conserved between *S. pombe* and *Homo sapiens*, based on the results of substrate mapping screen. Thick lines with arrowheads represent kinase-substrate relationships found in this study; their color indicates the kinase family: SR protein kinase (blue) and Cdc2-like kinase (red). Thin gray lines indicate known physical interactions. Node size reflects number of independent identifications of the substrate as a fraction of the total number of experiments. In cases in which multiple potential orthologs were found to be phosphorylated in *H. sapiens*, a representative example is shown.

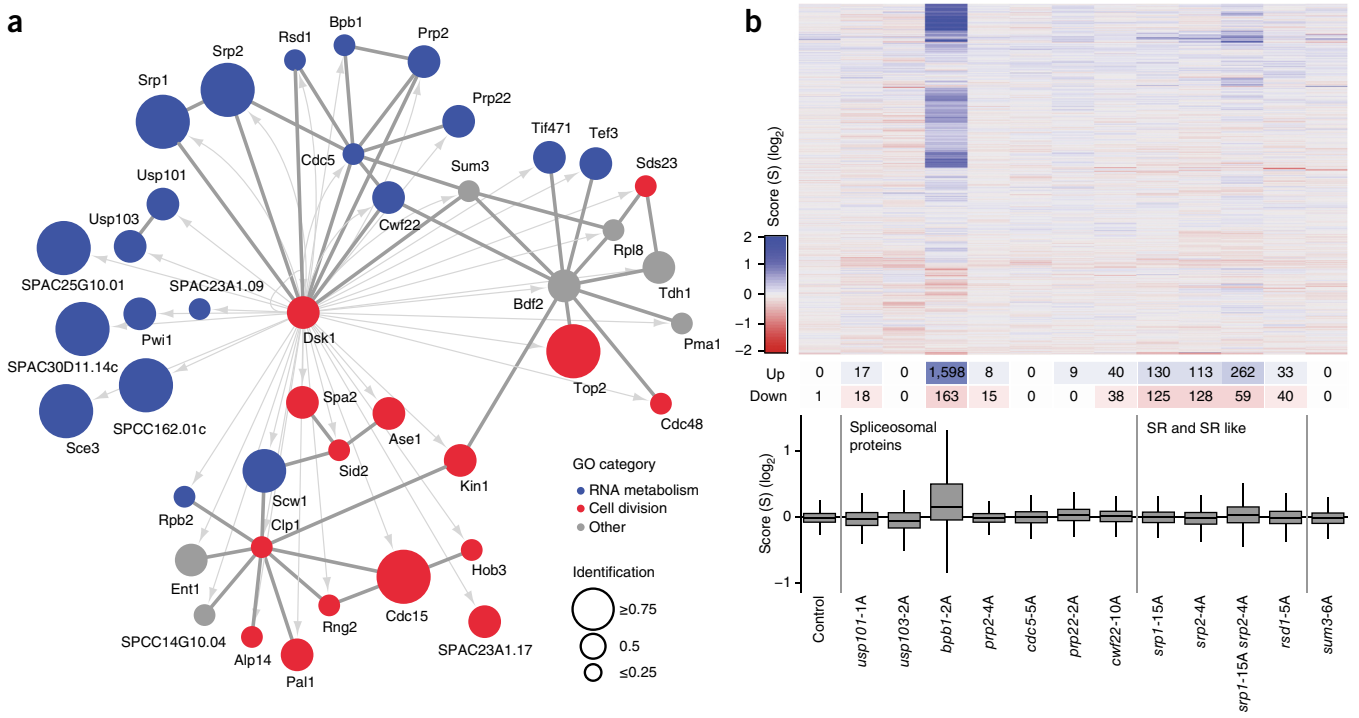

Figure 3 Dsk1 directly phosphorylates multiple essential RNA-splicing factors. (**a**) Network diagram of selected Dsk1 substrates. Physical interactions (thick gray lines) and kinase-substrate relationship between Dsk1 and the protein found in this study (thin gray lines with arrowhead) are shown. Gene ontology (GO) annotation of proteins is represented by color (blue, RNA splicing and related; red, cell division and related; gray, other). Node size reflects number of independent identifications of the substrate as a fraction of the total number of experiments. (**b**) Heat map (as in **Fig. 1b**) of hierarchical clustering of scores for each phosphorylation mutant. 1A–15A indicate the number of residues mutated to alanine. The control column is based on the same data used in **Figure 1b**.

particularly enriched in our data sets, thus suggesting an RXXSP consensus motif, in which XX often is SR. This motif is consistent with the established view that splicing kinases prefer phosphorylation of SR repeats, and it highlights the importance of a proline residue for substrate recognition[27]. We identified substrates of the human splicing kinase orthologs Srpk2 (**Supplementary Table 3**) and Clk1 (**Supplementary Table 4**) in HeLa extracts and found a similar preference for RXXSP (**Fig. 2c**,**d**), a result suggesting that this consensus motif is an evolutionarily conserved hallmark of substrate recognition by splicing kinases. We identified nine orthologous proteins that are direct substrates of splicing kinases in both fission yeast and human extracts. Remarkably, all of those proteins are involved in RNA processing and might constitute part of an evolutionarily conserved splicing kinase–phosphorylation network (**Fig. 2e**).

Substrate mapping reveals Bpb1 as an important Dsk1 target

We focused our efforts on validating the functional importance of kinase substrates on targets of Dsk1 because Dsk1 activity, but not Lkh1 activity, was required for efficient splicing of a large number of transcripts (**Fig. 1b**). Gene ontology–term enrichment analysis of Dsk1 substrates showed a significant enrichment of proteins involved in RNA splicing as well as in other RNA processing categories (**Supplementary Table 5**). To determine whether the list contained groups of functionally related proteins, we cross-referenced the substrates with known physical interactions. This analysis resulted in two connected clusters of substrates, which appeared to be functionally separated into proteins involved in RNA processing (for example, Cdc5, Prp2, Cwf22, Prp22, Bpb1, Rsd1, Srp1 and Srp2) and cell division (for example, Cdc15, Rng2, Ase1 and Clp1) (**Fig. 3a**). This finding is consistent with Dsk1 being a kinase that coordinates RNA splicing and progression through the cell cycle[28,29].

To assess which Dsk1 phosphorylation events were functionally important for RNA splicing, we selected 11 substrates with important roles in different steps of RNA splicing, generated alanine-substituted phosphorylation-mutant strains and monitored splicing with microarrays. We chose known RNA-processing factors: the spliceosomal proteins Usp101, Usp103, Bpb1, Prp2, Prp22, Cwf22 and Cdc5; the splicing regulators Srp1, Srp2 and Rsd1; and the translation-initiation RNA helicase Sum3 (Ded1) (**Table 1**). The phosphorylation sites to be mutated were selected either because they were identified in the substrate mapping screen directly or because they resided in identified

Table 1 Dsk1 substrates selected for generation of phosphorylation mutants

Group	*S. pombe*	*S. cerevisiae*	*H. sapiens*
Spliceosomal proteins	Usp101	Snp1	U1-70kD
	Usp103	Yhc1	U1-C
	Bpb1	Msl5	SF1
	Prp2	Mud2	U2AF65
	Cdc5	Cef1	CDC5
	Prp22	Prp22	DHX8
	Cwf22	Cwc22	CWC22
SR and SR like	Srp1	–	SRSF2
	Srp2	Npl3	SRSF5
	Rsd1	–	RBM39
Other	Sum3	Ded1	DDX3

Substrates are grouped on the basis of their known function; orthologs in *S. cerevisiae* and *H. sapiens* are listed.

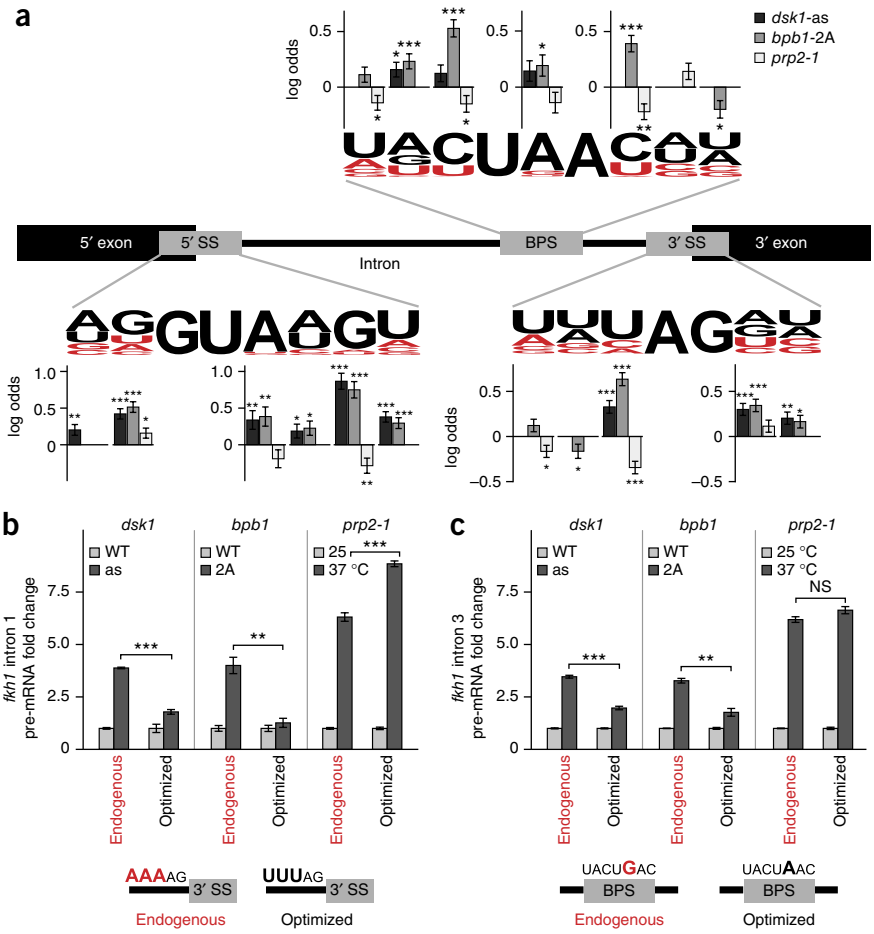

Figure 4 Dsk1 activity and Bpb1 phosphorylation are required for splicing of nonconsensus introns. (**a**) Schematic representation of *cis*-regulatory sequences at the 5′ SS, the branchpoint (BPS) and the 3′ SS, with their base composition in the *S. pombe* genome. The relative importance (in log odds) for classifying introns as significantly retained, on the basis of a logistic regression model, is analyzed for each nucleotide position within each *cis*-regulatory sequence. At each position, nucleotides are classified as rare (red) or common (black) according to their genome-wide frequency. Positive log odds at a given position for a given genotype indicate that rare nucleotides positively correlate with intron retention. Only contributions that were retained after stepwise model simplification are shown. Error bars, s.e.m. of logistic regression model (Online Methods). (**b**) Bar graphs of the fold enrichment of *fkh1* intron 1 pre-mRNA upon optimization of the 3′ SS, determined by RT-qPCR. Values are normalized to their respective controls. Error bars, s.e.m. ($n = 3$ cell cultures). NS, $P > 0.05$; $^{*}P < 0.05$; $^{**}P < 0.01$; $^{***}P < 0.001$ by two-sided Student's t test. (**c**) As in **b**, for *fkh1* intron 3 upon optimization of the BPS.

substrates and closely matched the RXXSP consensus motif. We expanded the list of substrates because the most common motif RSRSP is rich in arginine residues, which lead to variable trypsin cleavage and short peptides that are difficult to detect by MS. To our surprise, most phosphomutants had either no or, as in the case of the SR proteins Srp1 and Srp2, limited splicing defects (**Fig. 3b**). Combination of the two SR-protein mutants resulted in only a modestly increased splicing defect (**Fig. 3b** and **Supplementary Fig. 2a**). This suggests that most phosphorylation sites that we mutated were either redundant or not required for protein function under normal growth conditions. However, mutation of the conserved S131 and S133 residues to alanine in Bpb1 (denoted Bpb1-2A) caused significant intron retention in 1,598 introns (~35%) (**Fig. 3b**) and thus produces a defect quantitatively and qualitatively similar to inhibition of either Dsk1 ($\rho = 0.62 \pm 0.02$; $P < 10^{-6}$, two sided) or Prp4 ($\rho = 0.63 \pm 0.02$; $P < 10^{-6}$, two sided). An approximately nine-fold increase of unspliced *fkh1* intron 3 pre-mRNA relative to its isogenic controls in RT-qPCR confirmed the splicing defect of *bpb1*-2A (**Supplementary Fig. 2b**). We conclude that phosphorylation of the Dsk1 substrate Bpb1 has a major effect on the genome-wide splicing pattern.

Phosphoregulation assists in splicing of suboptimal introns

We were curious about why inhibition of Dsk1 and the Bpb1 phosphomutant compromised splicing of a subset of introns while not affecting others. To identify systematic trends of intron retention, we classified introns as being retained or not, on the basis of the microarray data, compiled information on the sequence features of each intron (**Supplementary Table 6**) and fit a logistic regression model. We found that intron features with noncanonical splice sites, such as rare nucleotides within the 5′ splice site (5′ SS), 3′ splice site (3′ SS) and branchpoint sequence (BPS) increased the probability of intron retention in inhibited *dsk1*-as and *bpb1*-2A strains (**Fig. 4a**). During early steps of spliceosome assembly, the RNA components of the U1 and U2 small nuclear ribonucleoproteins (snRNPs) directly interact with the 5′ SS and BPS, respectively. Retained introns on average had weaker interactions between the U1 small nuclear RNA (snRNA) and the 5′ SS as well as between the U2 snRNA and the BPS, as judged by the predicted free energy released by heteroduplex formation (**Supplementary Fig. 3a**). Importantly, introns retained in a temperature-sensitive mutant of the *S. pombe* U2AF^{65} ortholog *prp2* (*prp2-1*) (2,873 introns retained, ~62%) (**Supplementary Fig. 3b**) did not result in a consistent positive correlation with suboptimal *cis*-regulatory sequences (**Fig. 4a** and **Supplementary Fig. 3a**). These data suggest that weak splice sites are part of the signature that identifies introns that are more susceptible to phosphorylation-dependent regulation.

A key prediction of our computational analysis was that mutation of a suboptimal *cis*-regulatory sequence to an optimal sequence would make splicing of an intron less dependent on Dsk1 activity and Bpb1 phosphorylation. To test this, we replaced the endogenous suboptimal AAAAG 3′ SS sequence with the optimized UUUAG in intron 1 of the *fkh1* gene. As expected, *dsk1*-as and *bpb1*-2A strains showed significant intron retention in the presence of the endogenous 3′ SS. However, the optimized 3′ SS rescued intron retention almost completely in both genotypes (**Fig. 4b**). Similarly, replacement of the suboptimal BPS UACUGAC with the optimal UACUAAC sequence in *fkh1* intron 3 resulted in robust rescue of intron retention in *dsk1*-as and *bpb1*-2A strains (**Fig. 4c**). We observed no rescue of *fkh1* intron 1 and intron 3 splicing in the presence of optimized regulatory sequences in temperature-shifted *prp2-1* strains, a result

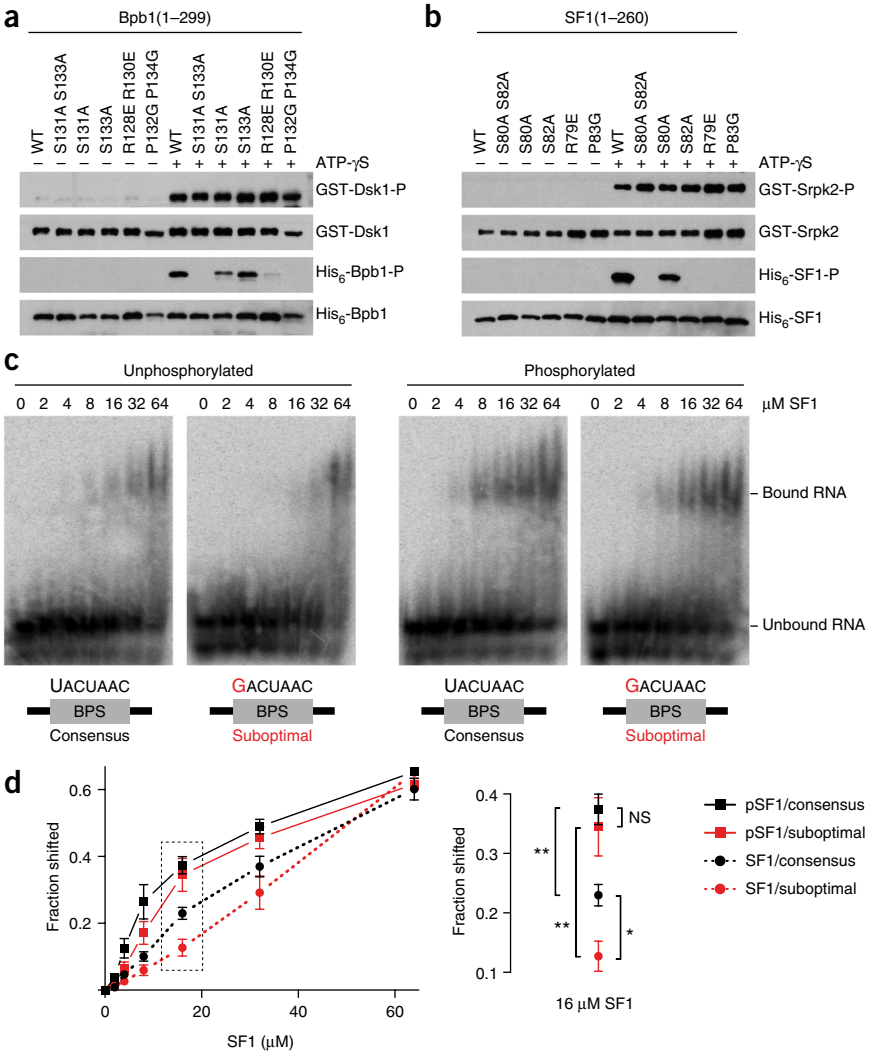

Figure 5 SF1 phosphorylation increases SF1 binding to nonconsensus introns. (**a**) Western blot of *in vitro* kinase assay analyzing Dsk1-dependent thiophosphorylation of constructs of the recombinant N-terminal fragment of Bpb1 (residues 1–299). Uncropped images are shown in **Supplementary Data Set 1**. His_6, hexahistidine tag. P denotes phosphorylated proteins. (**b**) As in **a**, for thiophosphorylation of various mutants of SF1(1–260) by recombinant Srpk2. (**c**) Native gel shift assays with unphosphorylated (left) or phosphorylated (right) versions of recombinant SF1(1–260) and U6 RNA with either a consensus (UACUAAC) or suboptimal (GACUAAC) branchpoint sequence. (**d**) Quantification of fraction of bound over total RNA at various concentrations of SF1. Error bars, s.e.m. ($n = 4$ independent experiments). Statistical significance testing of values at 16 µM SF1 (black box) are shown magnified, to the right of the main graph: NS, $P > 0.05$; $^*P < 0.05$; $^{**}P < 0.01$ by two-sided Student's t test.

indicating that improved splicing is not a general consequence of canonical splice sites but that it specifically mitigates the requirement for Dsk1 activity and Bpb1 phosphorylation (**Fig. 4b**,**c**). Optimization of the 5′ SS of *kes1* intron 5 also increased splicing relative to control, but this effect was not specific to *dsk1*-as and *bpb1*-2A strains (**Supplementary Fig. 3c**). Thus, the splicing kinase Dsk1 and phosphorylation of its substrate Bpb1 have an important *in vivo* role in assisting in the splicing of introns containing certain suboptimal *cis*-regulatory sequences.

Phosphorylation of SF1 increases binding to suboptimal BPS

The functionally important phosphorylation sites S131 and S133 within Bpb1 are embedded in two staggered RXXSP motifs, which have been highly conserved throughout evolution[30]. Because we had inferred phosphorylation of Bpb1 at S131 and S133 from the phosphorylation consensus motif, we validated that these two sites were indeed phosphorylated by Dsk1. Dsk1 readily phosphorylated WT Bpb1 *in vitro*, and mutation of Bpb1 at either S131 or S133 to alanine did not abolish phosphorylation (**Fig. 5a**). However, mutation of both S131 and S133 did, thus indicating that these two residues are the major sites of Bpb1 phosphorylation by Dsk1 (**Fig. 5a**). To test the importance of the R(−3) and P1 positions within the RXXSP motif, we replaced the two R(−3) positions with glutamate (R128E R130E) and the two P1 positions with glycine (P132G P134G). Both mutations prevented phosphorylation similarly to S131A S133A (**Fig. 5a**), a result validating the importance of the RXXSP motif and the essential nature of R(−3) and P1 for the recognition of substrates by Dsk1. Moreover, phosphorylation of the homologous residues S80 and S82 of SF1 depended on Srpk2 (**Fig. 5b**). Similarly to the case for Bpb1, mutation of the R(−3) and P1 within the RXXSP motif surrounding S82 resulted in complete loss of phosphorylation (**Fig. 5b**).

Recruitment of branchpoint-binding protein to RNA is an important early step of intron recognition in yeast and humans[31–38], and phosphorylation changes the ability of SF1 to bind RNA[30,39,40]. To elucidate the mechanism of how phosphorylation might assist in splicing of nonconsensus introns, we asked how phosphorylation of branchpoint-binding protein affected the protein's binding to RNA with optimal and suboptimal BPSs. Owing to difficulties in isolating sufficient quantities of pure Bpb1, we turned to its human ortholog SF1 for our mobility shift assays. Phosphorylation increased SF1 binding to consensus and nonconsensus RNA, yet the tighter binding was particularly dramatic in the case of RNAs with a nonconsensus BPS (P <0.05 at 16 µM) (**Fig. 5c**,**d**). Importantly, SF1's phosphorylation increased its binding affinity to similar levels for both consensus and nonconsensus RNAs. A different mutation in the canonical BPS had a similar effect (**Supplementary Fig. 4a**,**b**). This result suggests that phosphorylated branchpoint-binding protein masks the intrinsic strengths of BPSs and that regulation of kinase activity can dynamically modulate Bpb1 (SF1) binding to nonconsensus sequences, thus resulting in differential efficiency of RNA splicing *in vivo*.

DISCUSSION

The spliceosome is a complex molecular machine that carries out faithful recognition and removal of introns from pre-mRNAs. How the spliceosome accurately identifies introns of diverse sequence and length, and is additionally able to alter such recognition in response to signals, remains largely unanswered. Phosphorylation of the spliceosome and its regulators has been known to be an important modulator of spliceosome assembly and catalysis[13,41]. Using an

unbiased proteome-wide substrate mapping approach, we show that SR protein kinases use an evolutionarily conserved RXXSP phosphorylation motif to regulate components of the splicing machinery. This motif is consistent with phosphorylation of RS repeats, thus extending understanding of substrate recognition for this family of kinases[6]. In addition, proline has previously been shown to accelerate phosphorylation of Srsf1 by Srpk1 and Clk1 (ref. 27), and it has been demonstrated that Srpk1 processively phosphorylates RS repeats[42,43]. We speculate that P1 could facilitate the initial phosphorylation event, and then the kinase would subsequently switch to a processive mode, which has been suggested to fine-tune the localization and function of SR proteins[44–46].

The mapping of substrates of SR protein kinase in fission yeast and humans revealed a rich, partially conserved network of proteins involved in RNA metabolism and in other processes such as the cell cycle. The major splicing target of Dsk1 is the branchpoint-binding protein Bpb1, which Dsk1 phosphorylates on two evolutionarily conserved residues (S131 and S133) within two staggered RXXSP motifs. This dual-phosphorylation event is evolutionarily conserved because Srpk2 phosphorylates the corresponding residues S80 and S82 on the human Bpb1 ortholog SF1. Previously, the same residues of SF1 were reported to be phosphorylated by KIS kinase[39], and there is evidence that their phosphorylation depends on Prp4 (ref. 47). However, the functional impact of these phosphorylation events on RNA splicing remained unclear. Using microarrays, we show that both Dsk1 kinase activity and phosphorylation of Bpb1 on S131 and S133 are required for splicing of ~40% of introns in the *S. pombe* genome. The convergence of multiple kinases in the phosphorylation of two evolutionarily conserved phosphorylation sites further hints at the functional importance of these residues.

We demonstrate that the splicing efficiency of introns with nonconsensus splice sites was particularly compromised upon loss of Dsk1 activity or phosphorylation of Bpb1. The role of phosphorylation of Bpb1 refines the previous observations in budding yeast, in which depletion of the Bpb1 ortholog Msl5 led to reduced assembly of the commitment complex II (CC2)[48], and reporter transcripts with suboptimal BPSs displayed splicing defects[49]. By showing that SF1's phosphorylation increases its binding affinity for RNA with nonconsensus BPSs, we provide a mechanistic explanation for why suboptimal introns may be more susceptible to loss of Bbp1 function, which probably manifests as decreased splicing efficiency *in vivo* and slower spliceosome assembly *in vitro*.

Our work implies that diversification of splice sites from consensus sequences constitutes an important layer of flexibility in the modulation of splicing efficiency in response to phosphorylation by splicing kinases. Such a mechanism would explain how the expansion of splicing kinase families and the concomitant increased variability of *cis*-regulatory sequences in higher eukaryotes might help to establish alternative-splicing patterns specific to tissue type, developmental stage or environmental stimuli. SR protein kinases are particularly suited to relay such regulatory signals to the nucleus because their cellular localization depends on epidermal growth factor stimulation[22] and Akt[50].

METHODS

Methods and any associated references are available in the online version of the paper.

Accession codes. Raw microarray data have been deposited in the Gene Expression Omnibus database under accession code GSE62752.

Note: Any Supplementary Information and Source Data files are available in the online version of the paper.

ACKNOWLEDGMENTS

We thank J. Pleiss for designing the *S. pombe* splicing microarrays; N. Hertz, R. Levin and A. Burlingame for assistance with mass spectrometry; R. Freilich for assistance with strain construction; T. Tani (Kumamoto University) for providing us with the *prp2-1 S. pombe* strain; and M. Sattler (Technical University Munich) for the SF1 expression plasmid. We are grateful to D. Ruggero and members of the Guthrie and Shokat laboratories for helpful discussions and critical reading of the manuscript. Mass spectrometry was provided by the Bio-Organic Biomedical Mass Spectrometry Resource at University of California, San Francisco (A. Burlingame) supported by the Biomedical Technology Research Centers program of the US National Institutes of Health (NIH) National Institute of General Medical Sciences, 8P41GM103481. J.J.L. received a postdoctoral fellowship from the Jane Coffin Childs Memorial Fund for Medical Research. This work was supported by the Samuel Waxman Cancer Research Foundation (CA-0052023; K.M.S.) and NIH grants R01GM021119 (C.G.), F32GM101764 (M.C.M.) and R01AI094098 (K.M.S.). C.G. is supported as an American Cancer Society Research Professor of Molecular Genetics.

AUTHOR CONTRIBUTIONS

J.J.L. and M.C.M. designed, performed and analyzed the experiments. J.J.L., M.C.M., K.M.S. and C.G. wrote the manuscript.

COMPETING FINANCIAL INTERESTS

The authors declare no competing financial interests.

1. Wahl, M.C., Will, C.L. & Lührmann, R. The spliceosome: design principles of a dynamic RNP machine. *Cell* **136**, 701–718 (2009).
2. Mermoud, J.E., Cohen, P. & Lamond, A.I. Ser/Thr-specific protein phosphatases are required for both catalytic steps of pre-mRNA splicing. *Nucleic Acids Res.* **20**, 5263–5269 (1992).
3. Mermoud, J.E., Cohen, P.T. & Lamond, A.I. Regulation of mammalian spliceosome assembly by a protein phosphorylation mechanism. *EMBO J.* **13**, 5679–5688 (1994).
4. Tazi, J. *et al.* Thiophosphorylation of U1-70K protein inhibits pre-mRNA splicing. *Nature* **363**, 283–286 (1993).
5. Gui, J.F., Lane, W.S. & Fu, X.D. A serine kinase regulates intracellular localization of splicing factors in the cell cycle. *Nature* **369**, 678–682 (1994).
6. Ghosh, G. & Adams, J.A. Phosphorylation mechanism and structure of serine-arginine protein kinases. *FEBS J.* **278**, 587–597 (2011).
7. Giannakouros, T., Nikolakaki, E., Mylonis, I. & Georgatsou, E. Serine-arginine protein kinases: a small protein kinase family with a large cellular presence. *FEBS J.* **278**, 570–586 (2011).
8. Colwill, K. *et al.* The Clk/Sty protein kinase phosphorylates SR splicing factors and regulates their intranuclear distribution. *EMBO J.* **15**, 265–275 (1996).
9. Duncan, P.I., Stojdl, D.F., Marius, R.M., Scheit, K.H. & Bell, J.C. The Clk2 and Clk3 dual-specificity protein kinases regulate the intranuclear distribution of SR proteins and influence pre-mRNA splicing. *Exp. Cell Res.* **241**, 300–308 (1998).
10. Gross, T. *et al.* Functional analysis of the fission yeast Prp4 protein kinase involved in pre-mRNA splicing and isolation of a putative mammalian homologue. *Nucleic Acids Res.* **25**, 1028–1035 (1997).
11. Roth, M.B., Zahler, A.M. & Stolk, J.A. A conserved family of nuclear phosphoproteins localized to sites of polymerase II transcription. *J. Cell Biol.* **115**, 587–596 (1991).
12. Graveley, B.R. Sorting out the complexity of SR protein functions. *RNA* **6**, 1197–1211 (2000).
13. Zhou, Z. & Fu, X.-D. Regulation of splicing by SR proteins and SR protein-specific kinases. *Chromosoma* **122**, 191–207 (2013).
14. Cao, D.-S. *et al.* Large-scale prediction of human kinase-inhibitor interactions using protein sequences and molecular topological structures. *Anal. Chim. Acta* **792**, 10–18 (2013).
15. Xiao, S.H. & Manley, J.L. Phosphorylation of the ASF/SF2 RS domain affects both protein-protein and protein-RNA interactions and is necessary for splicing. *Genes Dev.* **11**, 334–344 (1997).
16. Xiao, S.H. & Manley, J.L. Phosphorylation-dephosphorylation differentially affects activities of splicing factor ASF/SF2. *EMBO J.* **17**, 6359–6367 (1998).
17. Cao, W., Jamison, S.F. & Garcia-Blanco, M.A. Both phosphorylation and dephosphorylation of ASF/SF2 are required for pre-mRNA splicing *in vitro*. *RNA* **3**, 1456–1467 (1997).
18. Tacke, R., Chen, Y. & Manley, J.L. Sequence-specific RNA binding by an SR protein requires RS domain phosphorylation: creation of an SRp40-specific splicing enhancer. *Proc. Natl. Acad. Sci. USA* **94**, 1148–1153 (1997).
19. Yeakley, J.M. *et al.* Phosphorylation regulates *in vivo* interaction and molecular targeting of serine/arginine-rich pre-mRNA splicing factors. *J. Cell Biol.* **145**, 447–455 (1999).

20. Roscigno, R.F. & Garcia-Blanco, M.A. SR proteins escort the U4/U6.U5 tri-snRNP to the spliceosome. *RNA* **1**, 692–706 (1995).
21. Boutz, P.L., Bhutkar, A. & Sharp, P.A. Detained introns are a novel, widespread class of post-transcriptionally spliced introns. *Genes Dev.* **29**, 63–80 (2015).
22. Zhou, Z. *et al.* The Akt-SRPK-SR axis constitutes a major pathway in transducing EGF Signaling to regulate alternative splicing in the nucleus. *Mol. Cell* **47**, 422–433 (2012).
23. Bishop, A.C. *et al.* A chemical switch for inhibitor-sensitive alleles of any protein kinase. *Nature* **407**, 395–401 (2000).
24. Inada, M. & Pleiss, J.A. Genome-wide approaches to monitor pre-mRNA splicing. *Methods Enzymol.* **470**, 51–75 (2010).
25. Hertz, N.T. *et al.* Chemical genetic approach for kinase-substrate mapping by covalent capture of thiophosphopeptides and analysis by mass spectrometry. *Curr. Protoc. Chem. Biol.* **2**, 15–36 (2010).
26. Colwill, K. *et al.* SRPK1 and Clk/Sty protein kinases show distinct substrate specificities for serine/arginine-rich splicing factors. *J. Biol. Chem.* **271**, 24569–24575 (1996).
27. Aubol, B.E. *et al.* Partitioning RS domain phosphorylation in an SR protein through the CLK and SRPK protein kinases. *J. Mol. Biol.* **425**, 2894–2909 (2013).
28. Tang, Z. *et al.* Interacting factors and cellular localization of SR protein-specific kinase Dsk1. *Exp. Cell Res.* **318**, 2071–2084 (2012).
29. Tang, Z., Yanagida, M. & Lin, R.J. Fission yeast mitotic regulator Dsk1 is an SR protein-specific kinase. *J. Biol. Chem.* **273**, 5963–5969 (1998).
30. Zhang, Y. *et al.* Structure, phosphorylation and U2AF65 binding of the N-terminal domain of splicing factor 1 during 3′-splice site recognition. *Nucleic Acids Res.* **41**, 1343–1354 (2013).
31. Krämer, A. & Utans, U. Three protein factors (SF1, SF3 and U2AF) function in pre-splicing complex formation in addition to snRNPs. *EMBO J.* **10**, 1503–1509 (1991).
32. Rain, J.C., Rafi, Z., Rhani, Z., Legrain, P. & Krämer, A. Conservation of functional domains involved in RNA binding and protein-protein interactions in human and *Saccharomyces cerevisiae* pre-mRNA splicing factor SF1. *RNA* **4**, 551–565 (1998).
33. Berglund, J.A., Abovich, N. & Rosbash, M. A cooperative interaction between U2AF65 and mBBP/SF1 facilitates branchpoint region recognition. *Genes Dev.* **12**, 858–867 (1998).
34. Berglund, J.A., Chua, K., Abovich, N., Reed, R. & Rosbash, M. The splicing factor BBP interacts specifically with the pre-mRNA branchpoint sequence UACUAAC. *Cell* **89**, 781–787 (1997).
35. Berglund, J.A., Fleming, M.L. & Rosbash, M. The KH domain of the branchpoint sequence binding protein determines specificity for the pre-mRNA branchpoint sequence. *RNA* **4**, 998–1006 (1998).
36. Huang, T., Vilardell, J. & Query, C.C. Pre-spliceosome formation in *S. pombe* requires a stable complex of SF1–U2AF(59)-U2AF(23). *EMBO J.* **21**, 5516–5526 (2002).
37. Liu, Z. *et al.* Structural basis for recognition of the intron branch site RNA by splicing factor 1. *Science* **294**, 1098–1102 (2001).
38. Jacewicz, A., Chico, L., Smith, P., Schwer, B. & Shuman, S. Structural basis for recognition of intron branchpoint RNA by yeast Msl5 and selective effects of interfacial mutations on splicing of yeast pre-mRNAs. *RNA* **21**, 401–414 (2015).
39. Manceau, V. *et al.* Major phosphorylation of SF1 on adjacent Ser-Pro motifs enhances interaction with U2AF65. *FEBS J.* **273**, 577–587 (2006).
40. Wang, W. *et al.* Structure of phosphorylated SF1 bound to U2AF65 in an essential splicing factor complex. *Structure* **21**, 197–208 (2013).
41. Stamm, S. Regulation of alternative splicing by reversible protein phosphorylation. *J. Biol. Chem.* **283**, 1223–1227 (2008).
42. Aubol, B.E. *et al.* Processive phosphorylation of alternative splicing factor/splicing factor 2. *Proc. Natl. Acad. Sci. USA* **100**, 12601–12606 (2003).
43. Ngo, J.C.K. *et al.* A sliding docking interaction is essential for sequential and processive phosphorylation of an SR protein by SRPK1. *Mol. Cell* **29**, 563–576 (2008).
44. Cho, S. *et al.* Interaction between the RNA binding domains of Ser-Arg splicing factor 1 and U1–70K snRNP protein determines early spliceosome assembly. *Proc. Natl. Acad. Sci. USA* **108**, 8233–8238 (2011).
45. Shin, C., Feng, Y. & Manley, J.L. Dephosphorylated SRp38 acts as a splicing repressor in response to heat shock. *Nature* **427**, 553–558 (2004).
46. Huang, Y., Gattoni, R., Stévenin, J. & Steitz, J.A. SR splicing factors serve as adapter proteins for TAP-dependent mRNA export. *Mol. Cell* **11**, 837–843 (2003).
47. Gao, Q. *et al.* Evaluation of cancer dependence and druggability of PRP4 kinase using cellular, biochemical, and structural approaches. *J. Biol. Chem.* **288**, 30125–30138 (2013).
48. Rutz, B. & Séraphin, B. Transient interaction of BBP/ScSF1 and Mud2 with the splicing machinery affects the kinetics of spliceosome assembly. *RNA* **5**, 819–831 (1999).
49. Rutz, B. & Séraphin, B. A dual role for BBP/ScSF1 in nuclear pre-mRNA retention and splicing. *EMBO J.* **19**, 1873–1886 (2000).
50. Jang, S.-W. *et al.* Interaction of Akt-phosphorylated SRPK2 with 14–3–3 mediates cell cycle and cell death in neurons. *J. Biol. Chem.* **284**, 24512–24525 (2009).

ONLINE METHODS

Strain construction. Fission yeast strains were constructed by direct one-step replacement of the endogenous gene with a linear cassette containing ~200 bp of the promoter, the mutated version of the gene, a C-terminal triple FLAG tag and an antibiotic-resistance cassette (KanR, NatR and HygR). Transformed strains were tested for expression of the tagged gene by western blotting with anti-FLAG (Sigma M2, cat. no. A8592; validation on manufacturer's website) and sequenced at the modified locus to confirm that the mutated version was introduced into the genome. The genotypes of all strains used in this study are available in **Supplementary Table 7**.

Detection of thiophosphorylation with western blotting. Thiophosphorylation in kinase assays and labeling experiments was detected by quenching of the phosphorylation reaction by addition of a final concentration of 30 µM EDTA and treatment with a final concentration of 2.5 mM *p*-nitrobenzyl mesylate (PNBM, dissolved at 25 mM in DMSO) for 30 min at room temperature. Alkylated thiophosphates were visualized with western blotting with an antibody raised to specifically detect thioesters.

Uncropped raw exposures of all western blot experiments are available in **Supplementary Data Set 1**. Proteins were detected with the following antibodies: thioesters (Epitomics, cat. no. 2686-1), His-tag (Qiagen, cat. no. 34660), GST tag (GE Healthcare, cat. no. RPN1236), TBP (Abcam, cat. no. ab51841) and β-actin (Abcam, cat. no. ab8227). Validation of antibody specificity is provided on the manufacturers' websites.

Protein expression. Full-length kinases were cloned into pGEX2T (N-terminal GST tag) and expressed in BL21. Protein expression was induced at an OD_{600} of 0.8 with 0.3 mM IPTG, and cells were grown for 16 h at 16 °C. Cells were lysed in 50 mM Tris-HCl, pH 7.4, 150 mM NaCl, 10% glycerol (v/v), 0.5 mM EDTA and 1 mM DTT by sonication in the presence of 1× Roche cOmplete protease inhibitors. Crude extracts were centrifuged at 30,000*g* for 30 min at 4 °C. The supernatant was incubated with glutathione-S-transferase agarose resin for 1 h at 4 °C, washed with lysis buffer containing 0.5 M NaCl and eluted with lysis buffer containing 20 mM glutathione, pH 7.4. Eluates were dialyzed twice against 20 mM HEPES, pH 7.9, 100 mM KCl, 10% glycerol (v/v), 0.2 mM EDTA and 1 mM DTT. N-terminally His_6-tagged fragments of Bpb1 (aa 1–299) and SF1 (aa 1–260) were purified from BL21 with the same growth and induction conditions as described for GST-tagged kinases. Lysis was performed in 50 mM Tris-HCl, pH 7.4, 0.5 M NaCl, 5% glycerol, 5 mM imidazole and 1 mM β-mercaptoethanol. Proteins were eluted in lysis buffer containing 250 mM imidazole. For gel shift assays, SF1 was further purified with gel filtration with 50 mM Tris-HCl, pH 7.4, 0.5 M NaCl and 1 mM β-mercaptoethanol.

Substrate mapping and analysis. For the preparation of fission yeast extract, we resuspended frozen cell pellets in 20 mM HEPES, pH 7.9, 100 mM KCl, 10% glycerol (v/v), 0.2 mM EDTA, 1 mM DTT and 1× Roche cOmplete protease inhibitors, added an equal volume of glass beads and disrupted cells with 4 × 30-s pulses in a bead beater with 1-min recovery on ice between the pulses. After removal of the glass beads, cells were centrifuged at 20,000*g* at 4 °C for 15 min. The supernatant was used as whole cell extract in the labeling reactions. Human HeLa cell extracts were prepared from HeLa whole cell pellets (CilBiotech) with the same procedure, except cells were disrupted by sonication instead of glass beads.

Labeling was performed in a reaction volume of 400 µl containing 3 mg protein extract, 20 mM HEPES, pH 7.9, 100 mM KCl, 3 mM GTP, 1 mM DTT, 300 µM ATP, ATP-γS analog (Dsk1 and SRPK2, 100 µM phenethyl-ATP-γS (BioLog, cat. no. P 026); Lkh1 and CLK1, 100 µM furfuryl-ATP-γS (BioLog, cat. no. F008)), and no kinase, WT recombinant kinase or analog-sensitive recombinant kinase (Dsk1 F166G, Srpk2 F166G, Clk1 F241G or Lkh1 T441G) at 1 µM. Each condition was run in duplicate for 90 min at room temperature. Thiophosphate-containing peptides were purified and eluted for MS as described previously[25].

Specific phosphopeptides were determined by subtractive filtering of phosphopeptide identified under no-kinase or WT-kinase conditions from analog-sensitive substrate lists. Consensus motifs were generated from specific phosphosites that were independently identified at least twice by a given kinase with IceLogo (http://iomics.ugent.be/icelogoserver/logo.html/). The cutoff for reported enrichment of amino acid residues was set to $P \leq 0.001$. Candidates for mutational analysis were sites either directly identified in the substrate-mapping screen or sites within identified target proteins closely matching the consensus motif derived from the substrate-mapping screen. Substrate networks were prepared by filtering lists of specific substrates by substrates with known physical interactions with other substrates in the list, on the basis of the BioGrid database (http://thebiogrid.org/), and displayed in Cytoscape (http://www.cytoscape.org/).

Microarray. Yeast strains were grown in rich YES5 medium to mid-log phase (OD_{600} 0.4–0.8) at 30 °C for non-temperature-sensitive strains. For *prp2-1*, yeast were grown at a permissive 25 °C temperature to mid-log phase and then were shifted to 37 °C for 2 h (ref. 51). For 3-BrB-PP1–treated kinase strains, *prp4* WT and *prp4*-as strains were grown to mid-log phase, and 10 µM of 3-BrB-PP1was added for 1 h. *dsk1* WT and *dsk1*-as strains were treated with 10 µM 3-BrB-PP1 for 8 h and harvested at mid-log phase. Cultures were collected by centrifugation and frozen at −80 °C. Sample preparation and microarray hybridization were performed as described previously[24]. Briefly, total RNA was isolated with hot-phenol extraction as outlined previously, and cDNA was synthesized with 500 U Superscript III (Invitrogen) for each reaction with 40 µg total RNA and 4 h incubation at 42 °C. All of the cDNA from control samples was labeled with Cy3 dyes, and all of the experimental samples were labeled with Cy5 dyes. Once samples were labeled, experiments were continued without interruption, and samples were kept exclusively in the dark. Appropriate Cy5 experimental and Cy3 control samples were combined. Samples were hybridized to Agilent custom 8,000 × 15,000 microarrays for 16 h at 60 °C in the dark with rotation.

Arrays were opened while submerged in Agilent Wash buffer I (Agilent) and were transferred to a rack and washed in wash buffer I while stirring for 1 min. Arrays were then transferred to wash buffer II at 37 °C for 1 min. Next, the arrays were transferred to acetonitrile for 1 min and finally to Stabilization & Drying Solution (Agilent) for 30 s. The arrays were then immediately scanned in an ozone-free chamber with a GenePix 4000B scanner (Molecular Devices). Scanning was carried out with GenePix software with 5-µm pixel size, two lines to average, and a focus position of 15. In order to get a balance between Cy5 and Cy3 fluorescent signals, we varied the ratio of the PMT for each wavelength until they were approximately equal, usually between 400 and 600. Some spots on the array were then flagged for oversaturation or spotty hydration with GenePix pro 7 software and excluded from analysis. Data were then normalized and analyzed as outlined below.

Microarray analysis. Each splicing event on the custom-designed splicing microarray was monitored with an exon probe reading out mRNA changes (E), an intron probe reading out unspliced pre-mRNA (I) and a splice-junction probe (J) reading out the junction between two spliced exons (**Supplementary Fig. 1d**). As expected, correlation between intron (I) and junction (J) signals was negative (for example, *dsk1*, $\rho = -0.19 \pm 0.02$ s.e.m.), whereas correlation between mRNA changes (E) and junction (J) signals was positive (for example, *dsk1*, $\rho = 0.46 \pm 0.01$ s.e.m.) (**Supplementary Fig. 1e**). We observed a weak positive correlation between mRNA changes (E) and intron (I) signals, probably because the exon probe also monitors pre-mRNA. To rule out a positive systematic contribution of gene-expression changes to the final score, we calculated the average contribution of gene expression to the score and found no consistent positive contribution of gene expression; if there was such a positive contribution, it was negligible in comparison to the average score for significantly changed splicing events (**Supplementary Fig. 1f**). We conclude that our calculation of an aggregate score is unlikely to introduce a major systematic bias into our analysis.

Microarrays were analyzed with the R package 'limma'[52]. Raw data were normalized by loess normalization. Statistically significant splicing events were determined by fitting of a linear model (lmFit) and subsequent adjustment of the variance with Bayesian hierarchical modeling (eBayes) and adjustment of the *P* values for multiple testing (FDR of 5%, Benjamini-Hochberg).

For fitting of a logistic regression model, we used the classification from our microarray data into introns that remained unchanged and significantly retained as the outcome variable. Intron features were compiled on the basis of the current fission yeast annotation of intron/exon boundaries (fungi_mart_22) with the R package 'biomaRt'[53]. Nucleotides at the 5′ SS, the branchpoint sequence and the 3′ SS were classified as common (all bases in descending order of frequency that make up 50% frequency on the basis of the genome at that position) or rare (all other nucleotides). The full model used all nucleotide positions for fitting and

doi:10.1038/nsmb.3057

was refined in a stepwise manner with the Akaike information criterion (AIC). Log odds and their standard errors from the final model are reported.

Calculation of free energy. Minimum free energy of the 5′ splice site and branch point sequences was estimated with RNAcofold in the ViennaRNA package[54]. The energy calculations are based on interaction of the 5′ splice site and the branchpoint sequence of introns to ACUUACCUG within the U1 snRNA and GUGUAGUA within the U2 snRNA[55]. Default parameters were used except for temperature, which was set to 33 °C, the optimal growth temperature of *S. pombe*. Energies are given in kcal/mol.

RT-qPCR. Cultures were grown, and RNA was extracted as described above for microarray analysis. For DMSO controls, an equal volume of DMSO was added in place of 3-BrB-PP1. 20 µg of total RNA was treated with 1 U of Turbo DNase (Ambion) for 1 h at 37 °C. RNA was precipitated with ethanol. 10 µg of resuspended DNase-digested RNA was then used as a template for reverse transcriptase. 2 µg dN9 random primer was annealed to RNA for 5 min at 60 °C in 50 mM Tris-HCl, pH 8.4, and 75 mM KCl; this was followed by a 5-min incubation on ice. Samples were split for treatment with or without reverse transcriptase as a control for genomic DNA contamination. Reverse transcription was carried out with 50 mM Tris-HCl, pH 8.4, 75 mM KCl, 2.5 mM $MgCl_2$, 10 mM DTT, 0.5 mM dNTPs and 0.5 µl 100× reverse transcriptase. Samples were incubated at room temperature for 15 min, incubated at 42 °C for 4 h and then diluted 1/12.5 in water. cDNA was diluted further (four- to ten-fold) depending on the qPCR amplicon. For qPCR analysis of cDNA, 250 nM dNTP, 1.5 mM $MgCl_2$, 200 mM each forward and reverse primers, 0.075× SYBR Green reagent (Sigma), 0.125 U BioReady rTaq and 1× BioReady rTaq Reaction Buffer (Bull Dog Bio) was used. qPCR was carried out with a Bio-Rad CFX96-C1000 thermocycler, and data were analyzed with Bio-Rad CFX Manager. To determine the fraction of spliced pre-mRNA, the ratio of two amplicons was taken with amplicons designed to span from intron into exon for pre-mRNA or within a single downstream exon for total RNA. The sequences of primers used in this study are available in **Supplementary Table 8**. Each experiment was done in triplicate ($n = 3$ independent cultures). Results were normalized to control, and differences were tested by two-sided Student *t* test.

Gel shift assay. RNA for gel shifts was purchased from Integrated DNA Technologies with HPLC purification. RNAs were derived from the native pre-U6 (SPSNRNA.06) intron from *S. pombe*. The branchpoint sequence is in bold lowercase, with the mutation from consensus in uppercase and the branch adenosine underlined. The 3′ SS is in italics. The sequences are GAGUCA**uacuaac**UCGUUGUUU*AG* (consensus; **Fig. 5c** and **Supplementary Fig. 4a**), GAGUCA**Gacuaac**UCGUUGUUU*AG* (suboptimal 1; **Fig. 5c**), and GAGUCA**uUcuaac**UCGUUGUUU*AG* (suboptimal 2; **Supplementary Fig. 4a**). 5′ labeling of RNA was carried out with [γ-32P]ATP and 10 U T4 polynucleotide kinase, per the manufacturer's directions (Thermo Scientific) for 1 h at 37 °C. Labeled RNA was purified on G-25 columns (GE Healthcare). Prior to gel shifts, 256 µM SF1(1–260) was incubated in 40-µl reactions for 18–19 h at 30 °C with 7 µM Srpk2 in 25 mM Tris-HCl, pH 7.5, 50 mM NaCl, 1 mM DTT, 150 mM $MgCl_2$ and 5% (v/v) glycerol in the presence or absence of 5 mM ATP. As a control, Srpk2 was also incubated in the same buffer without SF1 and in the presence or absence of 5 mM ATP. These kinase reactions were used immediately after overnight incubation in the gel shift assays. For gel shift assays, 3–7 nM RNA (500 c.p.m.) was incubated with the indicated amount of protein from the kinase reaction as well as 0.5 µg/µl *Escherichia coli* tRNA as a nonspecific competitor. Interactions were carried out in 10-µl reactions with 5 µl of the kinase reactions in 25 mM Tris, pH 7.5, 50 mM NaCl and 1 mM EDTA for 15 min at room temperature. Samples were then loaded in 0.5 TBE, 6% glycerol and 0.25% (w/v) bromophenol blue on 5% acrylamide gels (80:1 acrylamide/bisacrylamide) and separated at 4 °C for 3 h in 0.5× TBE at 150 V. Gels were then dried down and exposed to phosphor screens. Phosphor screens were scanned with a Typhoon 9400 imager (GE Healthcare) and quantified with ImageJ software (http://imagej.nih.gov/ij/).

51. Potashkin, J., Naik, K. & Wentz-Hunter, K. U2AF homolog required for splicing *in vivo*. *Science* **262**, 573–575 (1993).
52. Smyth, G.K. Linear models and empirical Bayes methods for assessing differential expression in microarray experiments. *Stat. App. Genet. Mol. Biol.* **3**, Article3 (2004).
53. Durinck, S. *et al.* BioMart and Bioconductor: a powerful link between biological databases and microarray data analysis. *Bioinformatics* **21**, 3439–3440 (2005).
54. Lorenz, R. *et al.* ViennaRNA Package 2.0. *Algorithms Mol. Biol.* **6**, 26 (2011).
55. Plass, M., Agirre, E., Reyes, D., Camara, F. & Eyras, E. Co-evolution of the branch site and SR proteins in eukaryotes. *Trends Genet.* **24**, 590–594 (2008).